Site-selective laser spectroscopy of Nd^{3+} ions in $0.8CaSiO_3$-$0.2Ca_3(PO_4)_2$ biocompatible eutectic glass-ceramics

D. Sola,[1] R. Balda,[1,2*] J.I. Peña,[3] and J. Fernández[1,2]

[1]*Materials Physics Center CSIC-UPV/EHU and Donostia International Physics Center, 20080 San Sebastián, Spain*
[2]*Departamento de Física Aplicada I, Escuela Técnica Superior de Ingeniería, Universidad del Pais Vasco UPV/EHU, Alda. Urquijo s/n 48013 Bilbao, Spain*
[3]*Instituto de Ciencia de Materiales de Aragón, Universidad de Zaragoza-CSIC, 50018 Zaragoza, Spain*
wupbacrr@bi.ehu.es

Abstract: In this work we report the influence of the crystallization stage of the host matrix on the spectroscopic properties of Nd^{3+} ions in biocompatible glass-ceramic eutectic rods of composition $0.8CaSiO_3$-$0.2Ca_3(PO_4)_2$ doped with 1 and 2 wt% of Nd_2O_3. The samples were obtained by the laser floating zone technique at different growth rates between 50 and 500 mm/h. The microstructural analysis shows that a growth rate increase or a rod diameter decrease leads the system to a structural arrangement from three (two crystalline and one amorphous) to two phases (one crystalline and one amorphous). Electron backscattering diffraction analysis shows the presence of Ca_2SiO_4 and apatite-like crystalline phases. Site-selective laser spectroscopy in the $^4I_{9/2}\rightarrow{}^4F_{3/2}/^4F_{5/2}$ transitions confirms that Nd^{3+} ions are incorporated in crystalline and amorphous phases in these glass-ceramic samples. In particular, the presence of Ca_2SiO_4 crystalline phase in the samples grown at low rates, which has an excellent in vitro bioactivity, can be unambiguously identified from the excitation spectra and lifetime measurements of the $^4F_{3/2}$ state of Nd^{3+} ions.

OCIS codes: (160.5690) Rare-earth-doped materials; (300.6360) Spectroscopy, laser; (160.1435) Biomaterials.

References and links

1. J. Llorca and V. M. Orera, "Directionally solidified eutectic ceramic oxides," Prog. Mater. Sci. **51**(6), 711–809 (2006) (and references therein).
2. R. I. Merino, J. A. Pardo, J. I. Peña, G. F. de la Fuente, A. Larrea, and V. M. Orera, "Luminescence properties of ZrO_2-CaO eutectic crystals with ordered lamellar microstructure activated with Er^{3+} ions," Phys. Rev. B **56**(17), 10907–10915 (1997).
3. R. Balda, S. Garcia-Revilla, J. Fernández, R. I. Merino, J. I. Peña, and V. M. Orera, "Near infrared to visible upconversion of Er^{3+} in $CaZrO_3$/CaSZ eutectic crystals with ordered lamellar microstructure," J. Lumin. **129**(12), 1422–1427 (2009).
4. P. N. de Aza, F. Guitian, and S. de Aza, "Phase diagram of wollastonite-tricalcium phosphate," J. Am. Ceram. Soc. **78**(6), 1653–1656 (1995).
5. P. N. De Aza, F. Guitián, and S. De Aza, "Bioeutectic: a new ceramic material for human bone replacement," Biomaterials **18**(19), 1285–1291 (1997).
6. P. N. De Aza, F. Guitian, and S. de Aza, "A new bioactive material which transforms *in situ* into hydroxyapatite," Acta Mater. **46**(7), 2541–2549 (1998).
7. M. Magallanes-Perdomo, P. Pena, P. N. De Aza, R. G. Carrodeguas, M. A. Rodríguez, X. Turrillas, S. De Aza, and A. H. De Aza, "Devitrification studies of wollastonite-tricalcium phosphate eutectic glass," Acta Biomater. **5**(8), 3057–3066 (2009).
8. M. Magallanes-Perdomo, Z. B. Luklinska, A. H. De Aza, R. G. Carrodeguas, S. De Aza, and P. Pena, "Bone-like forming ability of apatite-wollastonite glass ceramic," J. Eur. Ceram. Soc. **31**(9), 1549–1561 (2011).
9. C. Wang, Y. Xue, K. Lin, J. Lu, J. Chang, and J. Sun, "The enhancement of bone regeneration by a combination of osteoconductivity and osteostimulation using β-$CaSiO_3$/β-$Ca_3(PO_4)_2$ composite bioceramics," Acta Biomater. **8**(1), 350–360 (2012).

#165344 - $15.00 USD Received 23 Mar 2012; revised 17 Apr 2012; accepted 17 Apr 2012; published 24 Apr 2012

10. J. A. Pardo, J. I. Peña, R. I. Merino, R. Cases, A. Larrea, and V. M. Orera, "Spectroscopic properties of Er^{3+} and Nd^{3+} doped glasses with $0.8CaSiO_3$-$0.2Ca_3(PO_4)_2$ eutectic composition," J. Non-Cryst. Solids **298**(1), 23–31 (2002).
11. R. Balda, J. Fernández, I. Iparraguirre, J. Azkargorta, S. García-Revilla, J. I. Peña, R. I. Merino, and V. M. Orera, "Broadband laser tunability of Nd^{3+} ions in $0.8CaSiO_3$-$0.2Ca_3(PO_4)_2$ eutectic glass," Opt. Express **17**(6), 4382–4387 (2009).
12. R. Balda, R. I. Merino, J. I. Peña, V. M. Orera, and J. Fernández, "Laser spectroscopy of Nd^{3+} ions in glasses with the $0.8CaSiO_3$–$0.2Ca_3(PO_4)_2$ eutectic composition," Opt. Mater. **31**(9), 1319–1322 (2009).
13. M. J. Weber, "Science and technology of laser glass," J. Non-Cryst. Solids **123**(1-3), 208–222 (1990).
14. R. R. Jacobs and M. J. Weber, "Dependence of the $^4F_{3/2}\rightarrow{}^4I_{11/2}$ induced-emission cross section for Nd^{3+} on glass composition," IEEE J. Quantum Electron. **QE-12**, 102–111 (1976).
15. Z. Gou, J. Chang, and W. Zhai, "Preparation and characterization of novel bioactive dicalcium silicate ceramics," J. Eur. Ceram. Soc. **25**(9), 1507–1514 (2005).
16. D. Sola, F. J. Ester, P. B. Oliete, and J. I. Peña, "Study of the stability of the molten zone and the stresses induced during the growth of Al_2O_3–$Y_3Al_5O_{12}$ eutectic composite by the laser floating zone technique," J. Eur. Ceram. Soc. **31**(7), 1211–1218 (2011).
17. F. J. Ester, D. Sola, and J. I. Peña, "Efectos térmicos inducidos durante el crecimiento del compuesto eutéctico Al_2O_3-ZrO_2 (Y_2O_3) por fusión zonal con láser [Thermal stresses in the Al_2O_3-ZrO_2 (Y_2O_3) eutectic composite during the growth by the laser floating zone technique]," Bol. Soc. Esp. Ceram. Vidrio **47**, 352–357 (2008).
18. F. J. Ester and J. I. Peña, "Análisis de la zona fundida en el crecimiento del compuesto eutéctico Al_2O_3-ZrO_2 (Y_2O_3) por fusión zonal con láser [Analysis of the molten zone in the growth of the Al_2O_3-ZrO_2 (Y_2O_3) eutectic by the laser floating zone technique]," Bol. Soc. Esp. Ceram. Vidrio **46**, 240–246 (2007).
19. B. H. T. Chai, G. Loutts, J. Lefaucheur, X. X. Zhang, P. Hong, and M. Bass, "Comparison of Laser Performance of Nd-Doped YVO_4, $GdVO_4$, $Ca_5(PO_4)_3F$, $Sr_5(PO_4)_3F$ and $Sr_5(VO_4)_3F$," in *Advanced Solid-State Lasers,* Vol. 20 of 1994 OSA Proceedings Series (Optical Society of America, 1994), pp. 41–52.

1. Introduction

Eutectic ceramics are composite materials formed *in situ* from a melt. The development of eutectic ceramic composites has been of great interest because of the fine microstructure control that can be carried out by the solidification conditions. The alternation of two or more crystalline phases, joint at atomic level with micrometric spacing, lead to different geometries providing the material properties that depend on the nature of the phases. Directionally solidified eutectic ceramic oxides have been studied along the last decades due to their outstanding mechanical properties, microstructural stability, and corrosion resistance up to temperatures very close to their melting point which make them suitable for functional and structural purposes [1]. Furthermore, they can also be used for optical applications, since eutectics made from large optical band gap materials, such as insulator compounds, present the unusual characteristic of being at the same time a monolith and a multiphase material, and the optically active ions can be placed in different crystal field environments in the same material, as reported in ZrO_2–CaO eutectics activated with Er^{3+} ions [2,3].

The $CaSiO_3/Ca_3(PO_4)_2$ (W-TCP) eutectic composite presents two interesting properties: in the first place, it is a bioactive material since tricalcium phosphate (TCP), $Ca_3(PO_4)_2$, is osteoconductive and wollastonite (W), $CaSiO_3$, is bioactive with osteostimulative properties. The features, microstructure, bioactivity, biocompatibility, and *in vitro* and *in vivo* behaviors of this binary system have been widely studied, mainly in its glassy form [4–6]. Recent studies have focused on the devitrification process of this glass for obtaining glass-ceramic materials through thermal treatments to develop W–TCP implants with better bioactivity and improved mechanical properties [7–9]. In the second place, this eutectic glass has excellent optical properties. In particular, it was found that the lifetimes and emission cross-sections of the 1.06 μm (Nd^{3+}) and 1.5 μm (Er^{3+}) emissions in this glass are equivalent to those of the best commercially used alkaline-silicate glasses [10]. More recently, we have demonstrated laser emission under pulsed pumping which shows a behavior close to a Q-switch operation. Wavelength-resolved pump excitation of Nd^{3+} ions in this glass allows for a broad band tunability (10 nm) of the laser emission which is related with the variety of quasi-isolated crystal field site distributions of Nd^{3+} ions in this glass matrix [11,12].

Besides the interest of Nd^{3+} ions in the field of infrared (IR) optical amplification related with the radiative efficiency of the $^4F_{3/2}\rightarrow{}^4I_{11/2}$ emission, this ion can also be used as a probe for local ordering due to the close relation between its spectroscopic properties and the local structure and bonding at the ion site [13,14].

#165344 - $15.00 USD Received 23 Mar 2012; revised 17 Apr 2012; accepted 17 Apr 2012; published 24 Apr 2012

In this work we report, for the first time to our knowledge, the influence of the crystallization stage of the host matrix on the spectroscopic properties of Nd^{3+} ions in W-TCP eutectic glass-ceramics doped with 1 and 2 wt% of Nd_2O_3, grown by the laser floating zone (LFZ). This technique allows to grow rods and fibers at different growth rates directly from ceramic precursors as well as to incorporate doping ions. In addition, the number of phases, their size, and the alignment with respect to the growing direction can be modified by varying the grow rate (V) and/or rod diameter (D) of the samples. The performed microstructural analysis of the glass-ceramic samples shows the existence of three (two crystalline and one amorphous) or two phases (one crystalline and one amorphous) depending on the growth rate and rod diameter. The crystalline phases correspond to apatite-like ($Ca_{10}(PO_4)_6A$; A = O, $(OH)_2$) and Ca_2SiO_4 structures. The latter, which has attractive bioactive properties, is not observed in the glass-ceramics obtained through thermal treatments. Dicalcium silicate (Ca_2SiO_4) ceramics have shown an excellent *in vitro* bioactivity, since when immersed in simulated body fluid (SBF), a bonelike carbonate hydroxyapatite (CHA) layer is formed on their surface [15]. The results of the present work indicate that the transformation of this ceramic when soaked in SBF could be analyzed in vitro by using rare-earth ions as luminescence probes. Site-selective laser spectroscopy in the $^4I_{9/2} \rightarrow {}^4F_{3/2}/{}^4F_{5/2}$ transitions of Nd^{3+} ions have been used to investigate the crystal field changes felt by Nd^{3+} ions as a consequence of the sample crystallization stage. The differences among the spectral features of the site-selective excitation and emission spectra of Nd^{3+} ions allow to distinguish between crystalline and amorphous environment for the rare-earth ions and to correlate the spectroscopic properties with the microstructure of these eutectics.

2. Experimental

2.1. Samples fabrication

The precursor rods were obtained from the powder mixture of wollastonite and tricalcium phosphate in the eutectic 80% $CaSiO_3$, 20% $Ca_3(PO_4)_2$ mol% composition. Furthermore, 1 and 2 wt% of Nd_2O_3 were added to the eutectic composite to obtain the doped samples. The resulting powders were isostatically pressed at 200 MPa for 2 minutes to obtain ceramic rods which were sintered at 1200°C for 10 hours.

Glass-ceramic eutectic rods were obtained by the laser floating zone technique (LFZ). This technique has been described in detail elsewhere [1]. The laser floating zone system includes a 600 W CO_2 semisealed laser (Electronic Engineering Blade 600) emitting at 10.6 μm and an in-house built growth chamber with gold coated metal mirrors for beam focusing and two vertical axes for cylinder displacement. Both axes have independent rotation and translation movements. The mirror system inside the chamber consists of a reflaxicon that transforms the solid beam into a ring which is deflected by a flat mirror at 45° and focused on the ceramic rod by a parabolic mirror producing a homogenous heating. The correct optical alignment is obtained with the aid of a red diode laser coaxial with the infrared beam. Once the precursor is placed in the upper axis, the growth process starts by heating its lower end. When a drop is formed, a small seed placed in the lower axis is approached until a liquid bridge between the precursor and the seed is established. Then the seed is moved away while the precursor is moved towards the molten zone, and the volume of the liquid zone is kept constant. Identical feed and growth rates can be used when equal precursor and eutectic rod diameters are required. To increase or decrease the eutectic rod diameter, the growth rate must be lower or higher respectively than the precursor speed. The precursor and the grown rod are counter rotated to improve the heat distribution in the molten zone. This technique permits to control the solidification rate, providing high axial and radial thermal gradients in the liquid-solid interface, of paramount importance in the microstructure domain, and opens up the possibility of fabricating eutectic glasses and glass-ceramics [1]. The diameter of the rods and the growth rates were varied in order to modify the crystalline character of the samples. In the first place, maintaining constant the diameter around 2.5 mm, the samples were grown at rates of 50, 100, 250 and 500 mm/h. Secondly, while keeping the growth rate at 100 mm/h, the feed

#165344 - $15.00 USD Received 23 Mar 2012; revised 17 Apr 2012; accepted 17 Apr 2012; published 24 Apr 2012

rate was modified to obtain final diameters between 2.5 and 4.5 mm. Samples were grown in air, and after growth they were annealed at 650°C for 5 h to relieve inner stresses.

2.2. Characterization techniques

The microstructure and composition were determined by means of scanning electron microscopy (SEM) using a JEOL JSM6400 with EDX analysis, and Electron backscatter diffraction (EBSD) was carried out to determine the crystalline nature of the phases present in the samples by using a field emission JEOL JSM-7000F.

Site-selective steady-state emission and excitation spectra were obtained by exciting the sample with a Ti-sapphire ring laser (0.4 cm^{-1} linewidth) in the 770-920 nm spectral range. The sample temperature was varied between 10 and 300 K in a continuous flow cryostat. The fluorescence was analyzed with a 0.25 m Triax 190 monochromator, and the signal was detected by a Hamamatsu H10330A-75 photomultiplier and finally amplified by a standard lock-in technique.

Lifetime measurements were performed by exciting the samples with a Ti-sapphire laser, pumped by a pulsed frequency doubled Nd:YAG laser (9 ns pulse width), and detecting the emission with a Hamamatsu H10330A-75 photomultiplier. Data were processed by a Tektronix oscilloscope.

3. Results and discussion

3.1 Compositional and microstructural characterization

In first instance, the chemical composition of the glass-ceramics samples was analyzed to verify that the composition of the processed samples was around the eutectic point, 50.7 CaO + 31.0 SiO_2 + 18.3 P_2O_5 in wt%, and to check the amount of RE the samples were doped with. Table 1 shows the processing features of the glass-ceramic samples and the amount of oxides present in each sample. As can be seen, the composition of the samples as well as the

percentage of the doping material were close to the nominal value. Traces of Mg, Fe, and Al impurities were also found.

Table 1. Compositional analysis of the W-TCP eutectic glass-ceramics in wt% together with the growth rate (V) and diameter (D). The nominal composition is 1% Nd_2O_3 for samples 1-4 and 2% Nd_2O_3 for samples 5 and 6.

	V (mm/h)	D (mm)	SiO_2	P_2O_5	CaO	Nd_2O_3
Sample 1	50	2.50	29.50	18.92	51.57	0.91
Sample 2	100	2.30	31.06	18.50	50.44	0.90
Sample 3	250	2.60	31.31	18.30	50.38	1.02
Sample 4	500	2.45	30.89	18.61	50.50	1.08
Sample 5	100	2.45	31.17	18.51	50.32	1.83
Sample 6	100	4.50	31.75	18.00	50.24	2.05

In order to analyze the influence of the processing conditions on the microstructure of the glass-ceramic samples, a microstructural analysis was carried out by means of scanning electron microscopy (SEM). In the first place, the composites obtained after the laser floating process were analyzed. Figure 1 depicts the cross-section (Fig. 1(a)) and the longitudinal-section (Fig. 1(b)) of a directionally solidified sample grown at 100 mm/h, with a diameter of 2.5 mm, and doped with 1wt% of Nd_2O_3. The micrographs show how the microstructure is made up of fibers with an irregular shape, (clear phase), aligned parallel to the growing direction, embedded in a grayish matrix (dark and black phases).

#165344 - $15.00 USD Received 23 Mar 2012; revised 17 Apr 2012; accepted 17 Apr 2012; published 24 Apr 2012

The growth rate, rod diameter, and amount of doping material present in the sample are the key factors involved in the arrangement of the microstructure, i.e., in their size, number of phases, and alignment with respect to the growing direction. It is worth noticing that the axial and radial temperature gradients in the solidification interface are related to the cooling rate in such a way that the crystalline nature of the sample increases with diameter and decreases with growth rate [1,16–18]. As an example, Figs. 1(c) and 1(d) show the longitudinal-section micrographs of samples doped with 1 wt% of Nd_2O_3 with diameters around 2.5 mm, and grown at 50 mm/h (c) and 500 mm/h (d) respectively, whereas Figs. 1(e) and 1(f) show the longitudinal-section of samples doped with 2 wt% of Nd_2O_3 grown at 100 mm/h with diameters of 2.45 mm (e), and 4.5 mm (f) respectively. The inset in each micrograph shows the details of the microstructure in a cross-section view. These figures show how the variation in growth rate or diameter can modify the size as well as the number of phases present in the samples. A growth rate increase or a diameter decrease leads the system to a structural arrangement from three to two phases. In addition, by comparing the occupation areas for each phase the clear one diminishes between a 12 and a 32% and the dark phase increases between a 33 and a 79%. Furthermore, the parallel alignment of the phases with respect to the growing direction can be lost as the growth rate is diminished or the diameter increased as a consequence of the loss of flatness in the solidification front.

With regards to the amount of doping material, the disorder in the ceramic system increases with the addition of impurities to the eutectic composition and therefore, the capability of the atoms to be rearranged to produce the phases is slightly diminished. This effect can be observed by comparing samples grown with the same processing conditions but with different amounts of Nd_2O_3, see micrographs in Figs. 1(b) and 1(e). In this case, an increase in the amount of doping material leads to a diminution in the number of phases formed, which goes from three to two phases, and furthermore, the dark phase turns from crystalline into amorphous. Moreover, if the occupation areas of this phase were compared, around a 50% had been increased in the sample doped with a 2 wt% of Nd_2O_3 with respect to the one doped with 1 wt% of Nd_2O_3. In either case, the increase of doping material did not affect the alignment of the phases with respect to the growing direction.

An energy dispersive X-ray (EDX) analysis was carried out to determine the composition of the phases. In the case of samples with three phases, (samples 1, 2, and 6 from Table 1), the clear phase was rich in CaO and P_2O_5 with a low content of SiO_2. The dark phase was rich in SiO_2 and CaO with a very low content of P_2O_5, and in the black phase the amount of CaO and SiO_2 was high with a low content of P_2O_5. Regarding Nd_2O_3, though it was found in the three phases, both in the clear and dark ones with a similar content, it was mainly placed in the black phase. In the case of samples with two phases, (samples 3, 4, and 5 from Table 1), the composition of the clear and dark phases was similar to the previous case. As an example, Table 2 shows the compositional analysis in wt% of samples grown at 50 mm/h and 500 mm/h with a diameter around 2.5 mm and doped with 1wt% of Nd_2O_3.

Table 2. Compositional analysis in wt% of the phases present in the eutectic glass-ceramic samples grown at 50 mm/h and 500 mm/h and doped with 1wt% of Nd_2O_3

	V (mm/h)	SiO_2	P_2O_5	CaO	Nd_2O_3
Clear phase	50	15.54	31.67	52.17	0.61
Dark phase	50	50.18	3.18	46.11	0.53
Black phase	50	42.02	18.17	38.21	1.60
Clear phase	500	15.38	32.82	51.1	0.69
Dark phase	500	46.2	11.57	41.56	0.68

#165344 - $15.00 USD Received 23 Mar 2012; revised 17 Apr 2012; accepted 17 Apr 2012; published 24 Apr 2012

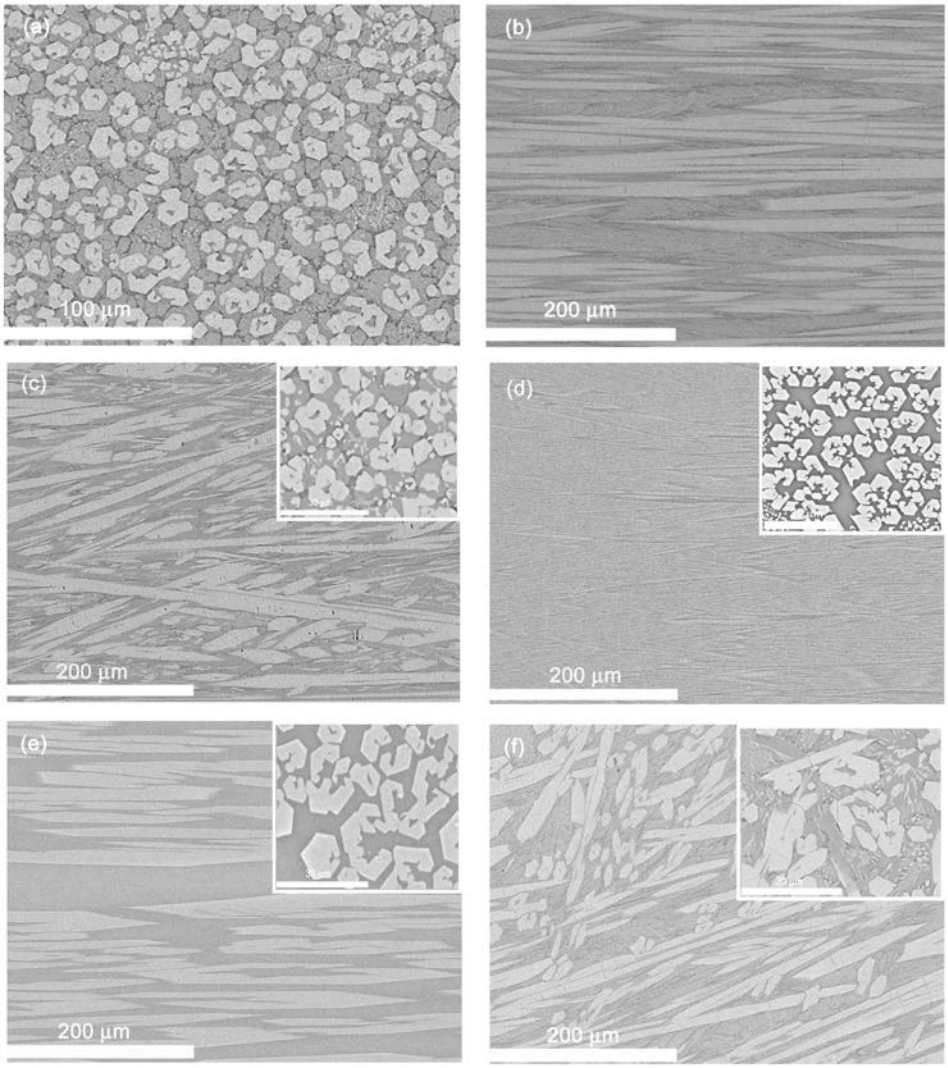

Fig. 1. Cross-section (a) and longitudinal-section (b) of a sample grown at 100 mm/h with a diameter of 2.5 mm and doped with 1 wt% of Nd_2O_3. Longitudinal-section micrographs of samples doped with 1 wt% of Nd_2O_3 with a diameter of 2.5 mm and grown at 50 mm/h (c) and 500 mm/h (d) and samples doped with 2 wt% of Nd_2O_3 grown at 100 mm/h with diameters 2.45 mm (e), and 4.5 mm (f). The inset in micrographs (c)-(f) shows the details of the microstructure in a cross-section view.

To ascertain the crystalline nature of the phases an electron backscatter diffraction (EBSD) analysis was performed in each sample. In the case of samples with three phases, the clear phase had an apatite-like structure, which could be apatite, oxyapatite or hydroxyapatite, while the dark phase had a Ca_2SiO_4 structure and the black one was amorphous. In the case of samples with two phases, the clear phase, as in the previous case, had an apatite-like structure but in this case the dark one was amorphous. Figure 2 shows the cross-section micrograph of a sample grown at 50 mm/h doped with 1wt% of Nd_2O_3. The insets show the electron backscatter diffraction patterns corresponding to an oxyapatite structure found in the clear phase, (1), and to the dicalcium silicate found in the dark phase, (2). Therefore, the clear phase was crystalline in any case but the dark one turned from crystalline into amorphous as the growth rate was increased or the diameter decreased.

#165344 - $15.00 USD Received 23 Mar 2012; revised 17 Apr 2012; accepted 17 Apr 2012; published 24 Apr 2012

Therefore, we can conclude that processing conditions and the amount of doping material play a key role in the crystallization process controlling the glassy character of the glass-ceramic samples. Furthermore, the features of this growing technique permit to obtain glass-ceramics starting from a non-equilibrium state and resulting in microstructures not reported so far in this system.

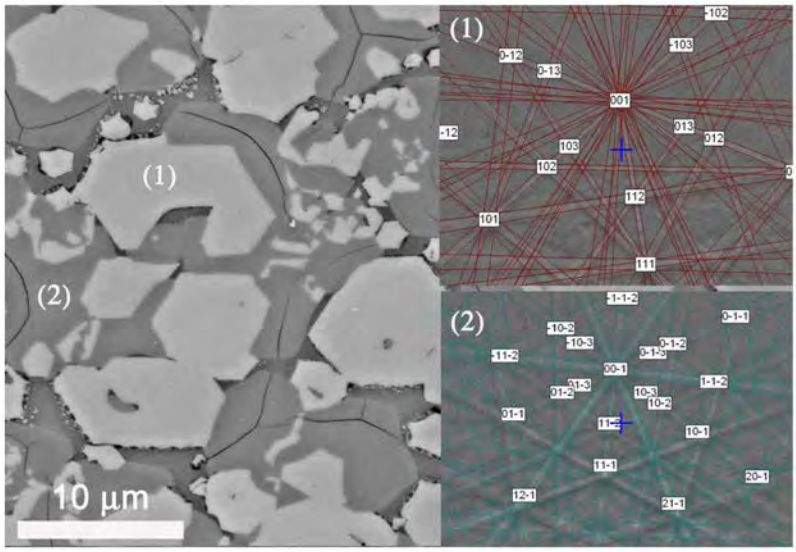

Fig. 2. Cross-section micrograph of a sample grown at 50 mm/h doped with 1 wt% of Nd_2O_3. The insets show the electron backscatter diffraction patterns corresponding to an oxyapatite structure, (1), and to the dicalcium silicate, (2).

3.2. Site-selective spectroscopy

To study the influence of the processing conditions on the spectroscopic properties of Nd^{3+} ions in the eutectic glass-ceramics we have performed site-selective excitation spectra of the $^4I_{9/2}\rightarrow{}^4F_{3/2,5/2}$ transitions collecting the luminescence at different emission wavelengths along the $^4F_{3/2}\rightarrow{}^4I_{11/2}$ laser transition for the glass-ceramics samples. Figure 3 shows the low temperature excitation spectra corresponding to the $^4I_{9/2}\rightarrow{}^4F_{3/2,5/2}$ transitions obtained at 1066 nm for the glass-ceramic samples doped with 1 wt% of Nd_2O_3 grown at 50, 100, 250, and 500 mm/h together with the excitation spectrum of the glass sample for comparison. The spectra corresponding to the $^4I_{9/2}\rightarrow{}^4F_{3/2}$ transition in the glass-ceramic samples show at least four main bands instead of the two ones associated with the two Stark components of the $^4F_{3/2}$ doublet in a low crystal field symmetry, which indicates the presence of different environments for Nd^{3+} ions in these matrices. By comparison with the excitation spectrum of the glass sample the spectra of this transition show two new peaks at around 859 and 886 nm. The spectra corresponding to the $^4I_{9/2}\rightarrow{}^4F_{5/2}$ transition also show a new sharp peak at around 810 nm, not observed in the excitation spectrum of the glass sample, which indicates that Nd^{3+} ions are in a crystalline environment. The position of these new peaks is almost independent of the growth rate. However, the ceramic/glassy character of the sample, which depends on the growth rate in this case, is in relation to the spectra obtained, in such a way that as growth rate decreases the spectrum becomes more defined with narrower peaks. These experimental results suggest that Nd^{3+} ions are incorporated in a crystalline phase in these glass-ceramics.

A similar behavior is obtained when the ceramic/glassy character of the sample is modified by the variations of the rod diameter. As in the previous case, the position of the bands corresponding to the $^4I_{9/2}\rightarrow{}^4F_{3/2,5/2}$ transitions is independent on the diameter of the rod

#165344 - $15.00 USD Received 23 Mar 2012; revised 17 Apr 2012; accepted 17 Apr 2012; published 24 Apr 2012

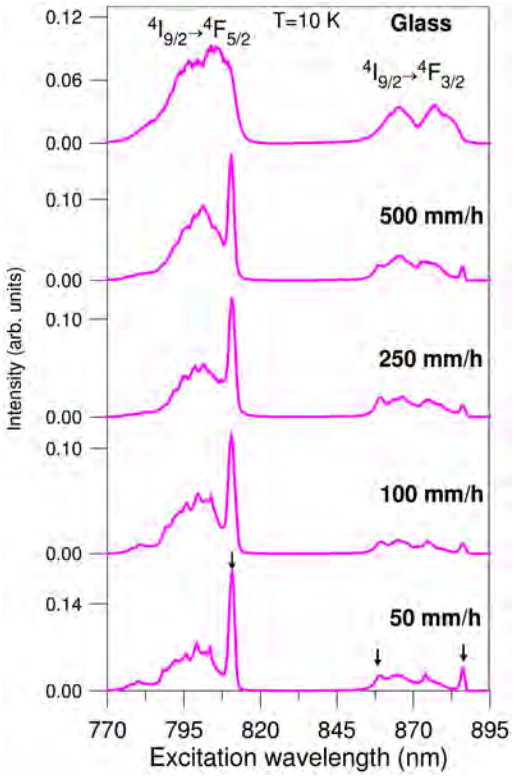

Fig. 3. Excitation spectra of the $^4I_{9/2}\rightarrow{}^4F_{5/2,3/2}$ transitions obtained by collecting the luminescence at 1066 nm in the glass and glass-ceramic samples obtained at different growth rates and doped with 1 wt% of Nd_2O_3.

and the spectrum is more defined with narrower peaks for the wider diameter, i.e., the more crystalline sample.

To obtain information about the different environments for Nd^{3+} ions in these glass-ceramic samples, excitation spectra at different emission wavelengths along the laser transition were performed. Figure 4(a) shows the excitation spectra obtained by collecting the luminescence at 1050, 1066, and 1080 nm of a sample obtained with a growth rate of 50 mm/h and doped with 1wt% of Nd_2O_3. The figure depicts how the spectrum is very different depending on the emission wavelength which indicates that Nd^{3+} ions are in different crystal field sites. The spectrum obtained at 1050 nm shows, for the $^4I_{9/2}\rightarrow{}^4F_{5/2}$ transition, sharp and well-resolved peaks with the most intense one located at around 802.2 nm which indicates a crystalline environment for Nd^{3+} ions. This intense peak disappears and the spectrum becomes an unstructured broad band for the samples grown at 250 and 500 mm/h (see Fig. 4(b) as an example). The low energy band corresponding to the $^4I_{9/2}\rightarrow{}^4F_{3/2}$ doublet narrows into one single component as expected for one well defined crystal field site. The high energy component of the doublet, which is more tightly coupled to the host vibrations, shows a more complex structure, probably due to the accidental mixing of emissions coming from different crystal field sites. Based on the previous microstructural analysis these results suggest that this spectrum corresponds to Nd^{3+} ions in a crystalline phase corresponding to Ca_2SiO_4 which is only present for samples grown at low rates (50 and 100 mm/h). However, the spectrum obtained at 1080 nm shows broad bands similar to those found in the glass sample. The spectrum corresponding to the $^4I_{9/2}\rightarrow{}^4F_{3/2}$ transition shows at least two components in the low energy band. This behavior has been also observed in the glass sample being a consequence of contributions from Nd^{3+} ions in a multiplicity of environments (see Fig. 4(c)). In the case of

#165344 - $15.00 USD Received 23 Mar 2012; revised 17 Apr 2012; accepted 17 Apr 2012; published 24 Apr 2012

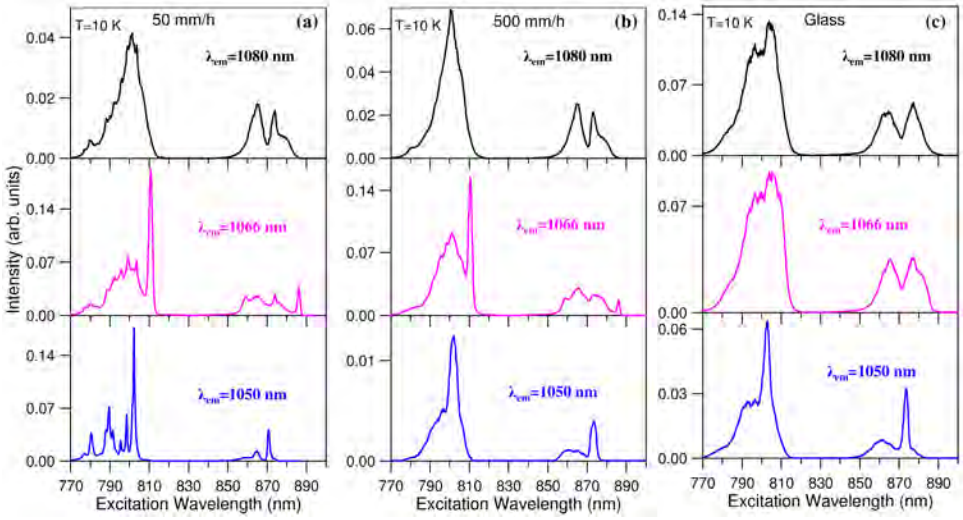

Fig. 4. Excitation spectra obtained at different emission wavelengths for the glass-ceramic samples grown at 50 mm/h (a) and 500 mm/h (b) and for the glass sample (c).

the excitation spectrum collected at 1066 nm, as seen before, in addition to the broad bands, sharp peaks at around 810.8, 859, and 886 nm appear which according to the EBSD analysis, could correspond to the apatite-like crystalline phase which is present in all glass-ceramics samples.

In order to confirm if the features shown by the excitation spectra can be definitely related to the existence of two crystalline phases and an amorphous one, we recorded the site-selective steady-state emission spectra for the $^4F_{3/2} \rightarrow {}^4I_{11/2}$ transition by exciting at 802.2 and 810.8 nm. Figure 5 shows the emission spectra at 10 K obtained under excitation at 802.2 (a) and 810.8 nm (b) respectively for the samples grown at 50 and 500 mm/h together with the spectra of the glass sample. As can be seen, different emission spectra are obtained depending on the excitation wavelength. The spectrum obtained for the glass-ceramic sample grown at 50 mm/h under excitation at 802.2 nm shows a complex structure with a sharp peak at 1050 nm together with other components. This peak disappears and the spectrum becomes broader and similar to the one found in the glass sample for the glass-ceramic grown at 500 mm/h. This indicates that at this wavelength, in the glass-ceramic samples grown at low rates (50 and 100 mm/h), we simultaneously excite Nd^{3+} ions in dicalcium silicate crystalline and in amorphous phases making it difficult to isolate the emission corresponding only to the crystalline phase. As we have mentioned before in the previous section, this crystalline phase becomes amorphous for the samples prepared with high growth rates which is confirmed by the features observed in the emission spectra of the samples grown at 250 and 500 mm/h.

However, the spectrum obtained at 810.8 nm shows, in all glass-ceramic samples, a sharp line with an effective linewidth of about 3.1 nm centered at around 1067 nm together with other much lower Stark components which suggests that at this wavelength we are exciting Nd^{3+} ions in a crystalline phase (see Fig. 5(b)). This phase corresponds to the apatite-like structure [19] which is present in all glass-ceramic samples.

The emission spectra obtained under excitation at different wavelengths along the $^4I_{9/2} \rightarrow {}^4F_{3/2}$ transition show a similar behavior but in this case it is more difficult to isolate the contribution from Nd^{3+} ions in different environments. Under excitation at 886.5 nm, the lowest energy peak of the $^4I_{9/2} \rightarrow {}^4F_{3/2}$ transition, the spectra are similar to those found at 810.8 nm, which indicates that these two peaks correspond to the same crystal field site. At other wavelengths, we simultaneously excite Nd^{3+} ions in crystalline and amorphous environments, and the spectra show a complex behavior.

#165344 - $15.00 USD Received 23 Mar 2012; revised 17 Apr 2012; accepted 17 Apr 2012; published 24 Apr 2012

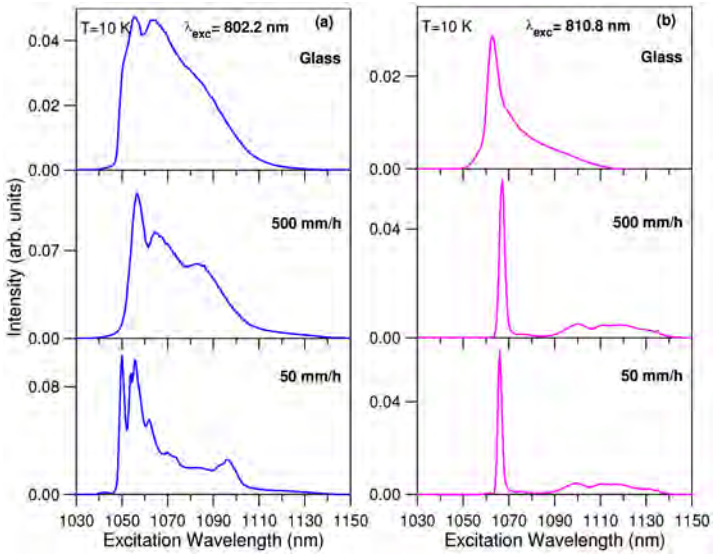

Fig. 5. Steady-state emission spectra of the $^4F_{3/2} \rightarrow {}^4I_{11/2}$ transition obtained under excitation at 802.2 nm (a) and 810.8 nm (b) for the glass-ceramic samples grown at 50 mm/h and 500 mm/h and for the glass sample.

Furthermore, the existence of different environments for Nd^{3+} ions is also reflected in the lifetimes of the $^4F_{3/2}$ state. Lifetime measurements of the $^4F_{3/2}$ state were performed by exciting the samples at 802.2 and 810.8 nm, and collecting the luminescence at different emission wavelengths in the $^4F_{3/2} \rightarrow {}^4I_{11/2}$ transition, corresponding to different sites observed in the steady-state emission spectra. If different sites for the rare-earth were present, the lifetime values should be dependent on the excitation and emission wavelengths. In our case, due to the spectral overlapping of the emission coming from Nd^{3+} ions in amorphous and crystalline environments, it is somewhat difficult to give accurate values for the excited state lifetime of each site. Only under excitation at 802.2 nm and collecting the luminescence at 1050 nm the decay is a single exponential with a lifetime of 590 μs for the glass-ceramic samples grown at low rates (50 mm/h and 100 mm/h). This value corresponds to the lifetime of Nd^{3+} ions in Ca_2SiO_4 crystalline phase. At other emission wavelengths the decays deviate from a single exponential and the lifetime value ranges between 272 μs and 171 μs depending on the excitation and emission wavelengths. As an example Fig. 6 shows the experimental

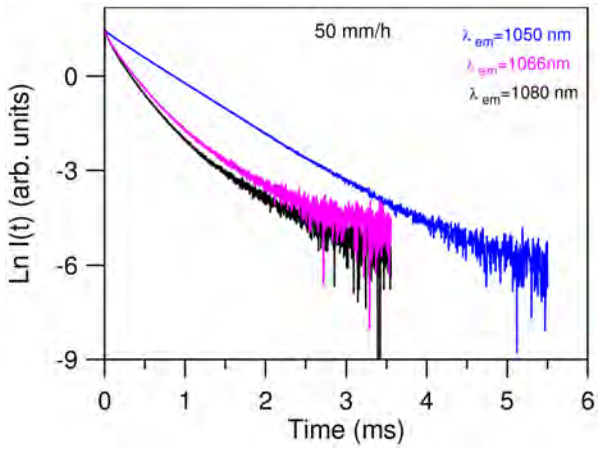

Fig. 6. Experimental decays of the $^4F_{3/2}$ level obtained under excitation at 802.2 nm at three emission wavelengths for the sample grown at 50 mm/h.

#165344 - $15.00 USD Received 23 Mar 2012; revised 17 Apr 2012; accepted 17 Apr 2012; published 24 Apr 2012

decays obtained by exciting at 802.2 nm and collecting the luminescence at 1050, 1066, and 1080 nm for the sample grown at 50 mm/h and doped with 1 wt% of Nd_2O_3.

In the case of samples grown at 250 and 500 mm/h, the decays are not single exponentials and the lifetimes display a variation from 220 μs to 153 μs as the excitation wavelength increases along the $^4I_{9/2} \rightarrow {}^4F_{5/2}$ transition. In the case of the glass sample this variation is from 279 to 205 μs and the decays can be described by a single exponential function, to a good approximation.

4. Conclusions

Directionally solidified eutectic glass-ceramics of composition $0.8CaSiO_3$-$0.2Ca_3(PO_4)_2$ doped with 1 and 2 wt% of Nd_2O_3 were fabricated by the laser floating zone technique. The features of this growing technique have enabled to obtain novel microstructures not reported so far in this system. The growth rate and rod diameter are the key factors involved in the crystallization process and hence in the size, number of phases present in the glass-ceramic samples, and in their alignment with respect to the growing direction. In particular, the glassy character of the glass-ceramic samples increases with the increase of the growth rate or the decrease of the rod diameter.

The microstructural analysis shows the existence of three (two crystalline and one amorphous) or two phases (one crystalline and one amorphous) depending on the growth rate. The crystalline phases correspond to Ca_2SiO_4 and apatite-like structures.

The differences among the spectral features of the site-selective excitation and emission spectra of Nd^{3+} ions allow to distinguish between crystalline and amorphous environments for the rare-earth ions and to correlate the spectroscopic properties with the microstructure of these eutectics. The presence of dicalcium silicate (Ca_2SiO_4) crystalline phase in the samples grown at low rates can be unambiguously identified from the excitation spectra and lifetime measurements of the $^4F_{3/2}$ state of Nd^{3+} ions.

These results show the potential applications of these materials obtained from the LFZ technique as luminescence bioprobes for in vitro applications and promote extended studies to other rare-earth ions which can be used in biomedical applications such as multicolor bioprobes and biosensors among others.

Acknowledgments

This work was supported by the Spanish Government MEC under Projects No. MAT2009-14282-C02-02, FIS2011-27968, Consolider SAUUL CSD2007-00013, and Basque Country Government (IT-331-07). Daniel Sola thanks the JAE-DOC program and the Science and Technology Inter-Ministry commission of Spain and FEDER funds of the EC under project MAT2009-13979-C03-03 for the financial support of his contract.

#165344 - $15.00 USD Received 23 Mar 2012; revised 17 Apr 2012; accepted 17 Apr 2012; published 24 Apr 2012